

UPPER TROPOSPHERIC WATER VAPOR FROM UARS MLS

W. G. Read, J. W. Waters, D. A. Flower, L. Froidevaux, and R. F. Jarnot
Jet Propulsion Laboratory, California Institute of Technology, Pasadena, CA.

D. L. Hartmann
University of Washington, Seattle, WA.

R. S. Harwood
University of Edinburgh, Edinburgh, UK

R. B. Rood
NASA/Goddard Space Flight Center, Greenbelt, MD.

Abstract

Initial results of upper tropospheric water vapor obtained from the Microwave limb Sounder (MLS) on the Upper Atmosphere Research Satellite (UARS) are presented. MLS is less affected by clouds than infrared or visible techniques, and provides daily near-global humidity monitoring. Best results are currently obtained when water vapor abundances are approximately 100-300 ppmv, corresponding to approximately 12 km height in the tropics and 7 km at high latitudes. The observed latitude variation of water vapor at 215 hPa is in good agreement with the UKUGAMP model. The ability to observe synoptic-scale features associated with tropopause height variations is clearly illustrated by comparison with the NASA GSFC assimilation model. Humidity dehydration streams extending from tropical convective regions are also observed.

1 Introduction

The global climate system is at the forefront of environmental concerns. Anthropogenic increases of greenhouse gases such as carbon dioxide could lead to enhancement of net downward radiative flux from the upper troposphere and a

warmer climate. Water vapor is the most important greenhouse gas (e.g. Manabe and Wetherald 1967; Houghton et al. 1990; Jones and Mitchell 1991) and the anticipated climate change arising from any increase in the anthropogenic greenhouse gases critically depends on the water vapor response to the additional radiation forcing. Assuming that the relative humidity remains unchanged, water vapor will amplify the climate response to changes in greenhouse gas concentrations, or to any other climate forcing. The water vapor content increases exponentially with increasing temperature for a constant relative humidity. The additional water can trap more radiation and cause further heating until a new equilibrium is established (Manabe and Wetherald 1967; Betts and Ridgway 1991). The positive feedback role of water vapor has been observed under clear sky conditions (Raval and Ramanathan 1989; Rind et al. 1991). Water vapor and cloud abundances are highly coupled, and cloud feedback varies considerably among current general circulation models (Cess et al. 1990). Although the climate sensitivity feedback associated with water vapor is generally believed to be strongly positive, it is possible that the combined effects of clouds, precipitation, dynamics, and water vapor may act as a net negative feedback system. Lindzen (1990) argues that increased surface temperature would increase convection which would dry the upper troposphere through subsidence. Based on cirrus cloud observations during an El Niño event, Ramanathan and Collins (1991) hypothesize that a runaway water vapor greenhouse effect over the warm oceans is checked by a negative feedback from increased reflectivity of upper tropospheric cirrus anvils formed from condensed moist air.

Evaluation of the relative importance of these effects has been hindered by a lack

of upper tropospheric humidity (UTH) data. Understanding the climate system requires global scale modeling, and global water vapor measurements are needed for validating general circulation model performance. The only practical method of obtaining continuous global data, is through satellite observations. Significant progress is being made to acquire this information. High horizontal and temporal resolution is now available from the Visible Infrared Spin Scan Radiometer (VISSR) Atmospheric Sounder (VAS) on the GOES geosynchronous satellites (Soden and Bretherton 1993; Udelhofen and Hartmann 1994). The High-Resolution Infrared Sounder (HIRS) is similar to VAS and operates on NOAA's polar orbiting platforms (Wu et al. 1993). HIRS sacrifices some temporal resolution but obtains full global coverage with one instrument. VAS and HIRS measurements are obscured by clouds, and both have limited vertical resolution: nominally a 300 hPa thick layer centered at 300 hPa altitude (the HIRS has two additional channels for middle and lower tropospheric humidity measurements). The Stratospheric Aerosol and Gas Experiment 11 (SAGE 11) makes water vapor measurements with ~ 1 km vertical resolution from the stratosphere to the ground or to the cloud tops (Rind et al. 1993). SAGE 11 uses solar occultation, which limits its measurements to about 30 per day, with approximately one month required to cover 70°S to 70°N (Cunnold et al. 1989).

The Microwave Limb Sounder (MLS) on the Upper Atmosphere Research Satellite (UARS), which has been in operation since late September 1991, gives a new capability for global UTH observations. Although not designed for this measurement, UARS MLS is sensitive to UTH when the field of view (FOV) of its CLO

spectral bands scanned down through the troposphere --- which happens once per minute on each limb scan. important features of the MLS measurement technique for UARS are its ability to observe through cirrus, near global coverage with over 1300 profiles per day, and an ability to determine vertical structure. The vertical resolution is limited by the instrument FOV which has a 3.0 km half-power gain width, and the best sensitivity to water vapor occurs in a vertical band where the abundance is ~ 150 ppmv, corresponding to ~ 12 km height at low latitudes and ~ 7 km at high latitudes. This paper describes some initial results obtained using a preliminary algorithm for extracting UTH from the MLS measurements.

2 Measurement Technique

The Microwave Limb Sounder (MLS) is a self-calibrating vertically-scanned limb sounding instrument that measures thermal emission in the millimeter-wavelength spectral region (Barath et al. 1993). UARS is in a circular 57° orbit, 585 km altitude, and MLS views the atmospheric limb in a direction perpendicular to the orbit path. There are 15 orbits per day and MLS makes a limb scan every 4.10 of orbit arc. Geophysical profiles are extracted from measurements made during each limb scan, which covers altitudes from the surface to 90 km. Calibration is performed on each limb scan. The orbital precession causes the measurement track longitude to move 5° , or 20 minutes earlier in local time over a 24 hour period. UARS makes a 180° yaw maneuver approximately every 36 days where MLS latitudinal coverage changes between 80°S to 34°N and 34°S to 80°N .

The MLS spectral band which gives ClO (e.g., Waters et al. 1993) measures

thermal radiation near 205 GHz frequency (wavelength ~ 1.5 mm), which is in a region free of any strong interfering lines in the stratospheric spectrum. When the FOV of this band is scanned down through the troposphere, the dominant contribution to its measured signal is thermal emission from water vapor. Water vapor can, in principle, be deduced from this measured signal over the vertical range between (1) where its signals are sufficiently strong to be distinguished from other effects, and (2) where its signals become so strong that they are optically thick and the measurements are mainly sensitive to atmospheric temperature. This range corresponds to water vapor abundances between approximately 100 and 300 ppmv. If the temperature profile is well known, the optically thick signal is a measure of relative humidity which is the principle used by the $6.7 \mu\text{m}$ channel on infrared sensors (e. g., Soden and Bretherton 1993). This can extend the MLS measurement capability lower into the troposphere, but is not considered here.

Altitude (pressure) registration of the measurements is obtained from observations of O_2 emission in the stratosphere (Waters 1993) extrapolated downward using hydrostatic equilibrium with temperatures from the operational analyses of the National Meteorological Center (NMC) and measured changes in the FOV pointing. Pointing, temperature and UARS platform attitude uncertainties correspond to 400 meters at 10-12 km (Fishbein et al., submitted to *J. Geophys. Res.* 1994). Figure 1 illustrates the concept for the simple retrieval scheme used for the initial results reported here. The radiance profile in the left panel is from a single limb scan near the tropics and shows the radiance increasing with decreasing altitude, corresponding to increasing atmospheric emission which is described by

an ‘absorption coefficient.’ The measurements have been vertically-interpolated onto an equal-spaced $\Delta \log_{10}$ pressure grid of 1/6 or approximately 2.5 km steps (the standard grid for UARS data). The plot also shows the corresponding atmospheric temperature profile from N MC. Good sensitivity to atmospheric absorption occurs before the radiance saturates, which is above 9 km for this measurement. The instrumental noise on each ‘2 second integration, for the channel used here, is <0.1 K equivalent brightness temperature which gives a signal to noise of greater than 1000:1 at the altitudes having best sensitivity. The radiance curve I_t in the left panel is modeled with the differential temperature radiative transfer equation (Read et al., in preparation),

$$I_t = \sum_{j=t+1}^N T_j^R \prod_{k=j}^N \delta_{kt} - \left(\prod_{k=t}^N \delta_{kt} \right) \times \left(\sum_{j=t+1}^N T_j^L \prod_{k=t}^{j-1} \delta_{kt} \right) \quad (1)$$

This equation is applied to an $N - 1$ layered atmosphere where each layer is separated by a surface with indices running from 1 (the Earth surface) to N (top of the $N - 1$ layer and non-absorbing space). The N levels correspond to the radiance measurement heights, which in this case have been interpolated from the actual measurements onto the standard UARS output grid as described above. Subscript t denotes the limb tangent surface and $i, j,$ and k indicate the surfaces used in the products and sums. $T_i^L = T_i^R = (T_{i-1} + T_{i+1})/2$ except when $i = N$ where $T_N^R = (T_{N-1} + T_N)/2$ and $T_N^L = T_N^R - T^s$. T_i , and T^s are the atmospheric brightness temperature (i.e. Planck radiation energy divided by the Boltzmann constant) at the i 'th surface and cosmic background respectively. δ_{it} is the layer transmission given by

$$\delta_{it} = \exp \{ -\alpha_i \Delta s_{it} \} \quad (2)$$

where α_i is the average absorption coefficient between surfaces i and $i+1$, and Δs_{it} is the path length between surfaces i and $i-1$ having a path geometry passing tangentially through surface t ($\delta_{Nt} \equiv 1$ and $\alpha_N \equiv ()$). Refraction is ignored here. Eqn. 1 can be recast into a recursion equation which yields a vertical profile of layer absorption coefficient using:

$$\alpha_t = \ln \left\{ \frac{\prod_{i=t+1}^N \delta_{it} \sum_{i=t+1}^N T_i^L \prod_{j=t+1}^{i-1} \delta_{jt}}{\sum_{i=t+1}^N T_i^R \prod_{j=i}^N \delta_{jt} - I_t} \right\} / (2\Delta s_{it}). \quad (3)$$

The center panel of Figure 1 shows the result of applying eqn. 3 to the radiance profile using the $A \log_{10} P \approx 1/6$ thick layers for each step. The FOV smearing is ignored in the simple procedure used here, which has the effect of degrading resolution and introducing biases. Also shown in the center panel is empirical dry atmosphere continuum emission (determined by us) which dominates the signal above the tropopause. This continuum emission is present in all MLS stratospheric radiances, and is nearly invariant with season and latitude (including the cold dry southern vortex), indicating that it is not caused by water vapor, clouds or aerosols. It is probably caused by collision-induced absorption (CIA) among nitrogen and oxygen molecules. Nitrogen CIA has been measured at other frequencies (Dagg et al. 1985) and theoretical estimates of its contribution are close to that observed (Borysow and Frommhold 1986). After subtracting the dry air CIA, the remaining absorption coefficient is interpreted as water vapor, using Liebe's (1989) millimeter-wave propagation model. The result is shown in the right panel of Figure 1.

Figure 1 also shows the calculated effects of ice on MLS 205 GHz measurements based on the theory given by Gunn and East (1954), and a dielectric model from Liebe et al. (1989). The MLS UHF measurements are at altitudes which can

be populated by cirrus anvils from deep convective towers. Measurements of ice crystals in cirrus anvils have revealed ice mass densities up to 0.1 g m^{-3} and particle sizes of 20-40 μm at temperatures $< 220 \text{ K}$ over spatial scales of 120 km (Knollenberg et al. 1993). This amount of ice could contribute $\sim 20\%$ to the total absorption coefficient at 12 km, as shown in Figure 1. In practice it will usually be less, because these are maximum values and not likely to be realized over the synoptic scales on which MLS makes measurements. The relative strengths of emission at 205 GHz due to water in ice:vapor:liquid are 1:2:100 for equal mass densities; lower altitude clouds containing liquid water $> 0.1 \text{ g/cm}^3$ (typical for a light cumulus cloud) will mask the vapor signal. Higher altitude polar stratospheric clouds and non-convective cirrus clouds are more than 30x less dense (typically $< 0.003 \text{ g m}^{-3}$ at $T < -40^\circ \text{ C}$ (Heymsfield and Platt 1984)) than tropical convective cirrus anvils and their effects on MLS water vapor measurements are negligible.

A test of the relative insensitivity to ice clouds is provided by MLS observations on 8 February 1993 through tropical cyclone "Oliver" over the Coral Sea. The particle microphysics in "Oliver" were characterized by aircraft experiments and reported by Puesche et al. (1994) who find very high ice densities in the range of 0.4- 1.0 g m^{-3} , and having a bimodal particle distribution with peaks of 0.04 and 0.4 μm at 10.7 km. They also found that particle concentrations increased with altitude up to 10.7 km. Based on Knollenberg et al. (1993) these conditions are up to ten times more severe than found in isolated convective systems. Shown in Figure 2 are three MLS measurement tracks at 215 hPa where the track indicated by stars goes through the cyclone and the other two tracks are adjacent and avoid

it. The latitudinal extent of the storm shown in the shading is based on the image in Figure 1 of Pueschelet et al. (1994). The MLS measurement track over "Oliver" detects humidification (relative to the two adjacent tracks) in a reasonable 80-90% range showing that the effect of this cyclone, if any, does not exceed 10-20% of the estimated mixing ratio. An unrealistically high value of 130% was measured immediately north of the storm and is not yet understood. Note that retrieved values on all three MLS measurement tracks increase to near 100% relative humidity in the tropics, as expected.

3 Some Initial Results

The initial MLS water vapor results shown here are for a 100 hPa thick layer centered at 215 hPa and assume no contribution from ice. It is difficult to validate the retrieved water vapor distribution against other measurements because of the lack of suitable datasets. Accordingly, a first evaluation is made by comparing the retrieved distribution with that anticipated from numerical simulation. Figure 3 shows simulated distributions from the UGAMP (UK Universities' Global Atmospheric Modelling Project) model (e.g., Gray et al. 1993). This is a spectral 19-level (hybrid sigma and p) model extending from the surface to 10 hPa, derived from the forecasting model of the European Centre for Medium-range Weather Forecasting. The runs utilized here were initialized with July conditions and the data for Fig. 3 were extracted 12 and 18 months into the run. These experiments utilized triangular-21 truncation, the Kuo convective scheme and specified sea surface temperatures corresponding to 1987 observations. Figure 3 shows individual

measurements and the zonal mean for a pair of days taken before and after a UARS flyaway in both January and July 1992. Results from the UGAMP model are also shown in the figure. MLS measurements show the expected latitude distribution of upper tropospheric water vapor, with maximum values occurring at the subtropics in the summer hemisphere. The measured zonal mean values are in reasonable agreement with UGAMP, except at high latitudes, where MLS values can be artificially high due to FOV effects which are not accounted for in the preliminary retrieval algorithms used here. The peak zonal value observed by MLS shows less displacement from the equator than the UGAMP model.

An interhemispheric asymmetry in UTII has been observed from aircraft *in situ* measurements by Kelly et al. (1991). They found the wintertime UTII poleward of 40° to be 50%, or 10 ppmv, drier in the southern hemisphere than in the northern hemisphere. The UGAMP results in Figure 3 also show this asymmetry. The MLS zonal average poleward of 40° also shows a ~ 10 ppmv drier southern hemisphere but with larger absolute values due to the unaccounted-for FOV effects. A definitive MLS statement regarding the wintertime asymmetry requires an improved retrieval algorithm currently being developed. The aircraft results were based on cloud-free data, whereas the MLS results have not been filtered for clouds.

Upper tropospheric water vapor measurements in the tropical West Pacific were made during the NASA Pacific Exploratory Mission West-A (PEMWA) during September-October 1991 using a Lyman- α instrument on a DC-8 aircraft (Kelly et al. 1993). Near-coincident MLS measurements have been compared with the PEMWA measurements and reasonable good agreement is obtained (Newell et al.,

submitted to *J. Geophys. Res., PEMWA Special Issuc* 1994). The MLS measurements also show a distribution of UTH which is consistent with the Walker circulation and its seasonal variation (Newell et al., submitted to *J. Geophys. Res.* 1994).

A demonstration of the MLS ability to track synoptic scale UTH features is shown in Figure 4. This figure compares an MLS 215 hPa water vapor map with a tropopause pressure map produced by the NASA GSFC data assimilation model (Schubert et al. 1993). Both maps are for 14 March 1993 when the US east coast was experiencing a severe blizzard. Note the good correlation between the dry and the low altitude (high pressure) tropopause regions. Conversely, the high altitude tropopause (above 215 hPa) is accompanied by wet tropospheric air. The clash between the tropospheric and stratospheric air along the east coast as shown in the GSFC assimilation map is clearly indicated in the MLS map by a sharp water vapor gradient. Other notable features are the arm of high tropopause pressure with dry air extending northwest from Hawaii, and the unusually low pressure tropopause and wet region occurring north of the Chukchi Sea.

Comparisons between fractional area coverage by high (above 440 hPa) and optically thick (visible optical depth greater than 9.38) clouds and the MLS and upper tropospheric, water distribution are shown in Figures 5 and 6. The cloud cover maps are the 1983- 1990 climatology and indicate the regions where deep convective clouds are prevalent. These are derived from the International Satellite Cloud Climatology Project C] data set (Rossow and Schiffer 1991; Hartmann and Ockert-Bell, 1992). The MLS upper tropospheric water distributions were obtained

by averaging all usable data from 1991 to 1994, and represent our first attempt at a climatology of tropospheric water vapor from MLS. Although the cloud and UT11 maps are for different years, the correspondence is good, as expected since convective areas occur in the same general region from year to year. The MLS maps clearly show detrainment streams extending from the convective (cloudy) regions. The divergence of water vapor from tropical convective zones is important to determine because the outgoing longwave radiation, and hence the global greenhouse budget, critically depend on it.

4 Future Work

The initial results shown here indicate MLS can provide information on global upper tropospheric water vapor. Future work will include development of a more sophisticated algorithm to provide useful quantitative values, and validation of the resulting product. A next-generation MLS is now being developed for NASA's Earth observing System (EOS). It will continue the UARS upper tropospheric water measurements to provide a long term record, and will also have enhanced capability to include complete coverage of water vapor from the upper tropopause through the stratosphere. Such measurements, hopefully, will advance our knowledge of Earth's climate system and the potential for changes in it.

Acknowledgements. We thank Mark Schoeberl (UARS Project Scientist) for encouraging us to pursue the MLS upper tropospheric water vapor measurement capability. The research described here done at the Jet Propulsion Laboratory, California Institute of Technology, was under contract with the National Aeronautics and Space Administration and funded through

its UARS project. Support for DLH was provided by NASA grant NAGW-2633 and NERC provided support for the UKUGAMP calculations by RSH.

References

- Barath, F., M. Chavez, R. Cofield, D. Flower, M. Frerking, M. Gram, W. Harris, J. Holden, R. Jarnot, W. Kloezeman, G. Klose, G. Lau, M. Loo, B. Maddison, R. Mattauach, R. McKinney, G. Peckham, H. Pickett, G. Siebes, F. Soltis, R. Suttie, J. Tarsala, J. Waters, and W. Wilson, 1993: The Upper Atmosphere Research Satellite Microwave Limb Sounder Instrument, *J. Geophys. Res.*, vol. 98, pp. 10751-10762.
- Betts, A. K. and W. Ridgeway, 1989: Climatic Equilibrium of the Atmospheric Convective Boundary Layer over a Tropical Ocean, *J. Atmos. Sci.*, vol. 46, pp. 2621-2641.
- Borysow, A and L. Frommhold, 1986: Collision-Induced Rotational Absorption Spectra of N₂-N₂ Pairs for Temperatures From 50 to 300K, *Astrophys. J.*, vol. 311, pp. 1043-1057.
- Cess, R. D., G. L. Potter, J. P. Blanchet, G. J. Boer, A. D. Del Genio, M. Déqué, V. Dymnikov, V. Galin, W. L. Gates, S. J. Ghan, J. "J". Kiehl, A. A. Lacis, H. Le Treuet, Z.-X. Li, X.-Z. Liang, B. J. McAvaney, V. P. Meleshko, J. F. B. Mitchell, J.-J. Morcrette, D. A. Randall, L. Rikus, P. Roeckner, J. F. Royer, U. Schleese, D. A. Sheinin, A. Slingo, A. P. Sokolov, K. E. Taylor, W. M. Washington, R. T. Wetherald, I. Yagai, and M.-H. Zhang, 1990: Intercomparison and Interpretation of Climate Feedback Processes in 19 Atmospheric General Circulation Models, *J. Geophys. Res.*, vol. 95, pp. 16601-16616.

- Cunnold, D. M., W. 1'. Chu, R. A. Barnes, M. P. McCormick, and R. E. Veiga, 1989: Validation of SAGE II Ozone Measurements, *J. Geophys. Res.*, vol. *94*, pp. 8447-8460.
- Dagg, I. R., A. Anderson, S. Yan, W. Smith, and L. A. A. Read, 1985: Collision-induced Absorption in Nitrogen at Low Temperatures, *Can. J. Phys.*, vol. *63*, pp. 625-631.
- Gray, I. J., M. Blackburn, M. F. Chipperfield, J. D. Haigh, D. R. Jackson, K. 1'. Shine, J. Thuburn, and W. Zhong, 1993: First Results from a 3-Dimensional Middle Atmosphere Model, *Adv. Space Res.*, vol. *13*, pp. 363-372.
- Gunn, K. L. S. and 1'. W. R. East, 1954: The Microwave Properties of Precipitation Particles, *Quart. J. Royal Meteorol. Soc.*, vol. *80*, pp. 522-545.
- Hartmann, D. L., M. B. Ockert-Bell, and M. . Michelson, 1992: The Effect of Cloud Type on Earth's Energy Balance: Global Analysis, *J. Climate*, vol. *5*, pp. 1281-1304.
- Heymsfield, A. J. and C. M. R. Platt, 1984: A Parameterization of the Particle Size Spectrum of Ice Clouds in Terms of the Ambient Temperature and the Ice Water Content, *J. Atmos. Sci.*, vol. *41*, pp. 846-855.
- Houghton, J. 1', G. J. Jenkins, and J. J. Ephraums, eds., 1990: *Climate Change. The IPCC Scientific Assessment*, 365 pp., Cambridge University Press, Cambridge.
- Jones, R. 1., and J. F. B. Mitchell, 1991: Is Water Vapour Understood?, *Nature*, vol. *353*, pp. 212.

- Kelly, K. K., A. F. Tuck, and J. Davies, 1991: Wintertime Asymmetry of Upper Tropospheric Water Between the Northern and Southern Hemispheres, *Nature*, vol. 353, pp. 244-247.
- Kelly, K. K., M. H. Proffitt, K. R. Chan, M. Loewenstein, J. R. Podolske, S. E. Strahan, J. C. Wilson, and D. Kley, 1993: Water Vapor and Cloud Water Measurements over Darwin during the STEP 1987 Tropical Mission, *J. Geophys. Res.*, vol. 98, pp. 8713-8723.
- Knollenberg, R. G., K. Kelly, and J. C. Wilson, 1993: Measurements of High Number Densities of Ice Crystals in the Tops of Tropical Cumulonimbus, *J. Geophys. Res.*, vol. 98, pp. 8639-8664.
- Liebe, H. J., 1989: MPM-An Atmospheric Millimeter-Wave Propagation Model, *Int. J. IR and MM Waves*, vol. 6, pp. 631-650.
- Liebe, H. J., T. Manabe, and G. A. Hufford, 1989: Millimeter-Wave Attenuation and Delay Rates Due to Fog/Cloud Conditions, *IEEE Trans. Antennas Propagat.*, vol. 37, pp. 1617-1623.
- Lindzen, R. S., 1990: Some Coolness Concerning Global Warming, *Bull. Amer. Meteor. Soc.*, vol. 71, pp. 288-299.
- Manabe, S. and R. T. Wetherald, 1967: Thermal Equilibrium of the Atmosphere with a Given Distribution of Relative Humidity, *J. Atmos. Sci.*, vol. 24, pp. 241-259.

- Peuschel, D. A., D. A. Allen, C. Black, S. Paisant, G. V. Ferry, S. D. Howard, J. M. Livingston, J. Redemann, C. E. Sorenson, and S. Verma, 1994: Condensed Water in Tropical Cyclone "Oliver", 8 February 1993, *Atmos. Res.*, in press.
- Ramanathan, V., W. Collins, [W]: Thermodynamic Regulation of Ocean Warming by Cirrus Clouds Deduced From Observations of the 1987 El Niño, *Nature*, vol. 351, pp. 27- 32.
- Raval, A. and V. Ramanathan, 1989: Observational Determination of the Greenhouse Effect, *Nature*, vol. 342, pp. 758-761.
- Rind, D., E.-W. Chiou, W. Chu, S. Oltmans, J. Lerner, J. Larsen, M. P. McCormick, and L. McMaster, 1993: Overview of the Stratospheric Aerosol and Gas Experiment 11 Water Vapor Observations: Method, Validation], and Data Characteristics, *J. Geophys. Res.*, vol. 98, pp. 4835-4856.
- Rind, D., E. W. Chiou, W. Chu, J. Larsen, S. Oltmans, J. Lerner, M. P. McCormick, and L. McMaster, 1991: Positive Water Vapour Feedback in Climate Models Confirmed by Satellite Data, *Nature*, vol. 349, pp. 500-503.
- Rossow, W. B., and R. A. Schiffer, 1991: ISCCP Cloud Data Products., *Bull. Amer. Meteor. Soc.*, vol. 72, pp. 2-20.
- Schubert, S. D., R. B. Rood, and J. Pfendner, 1993: An Assimilated Dataset for Earth Science Applications, *Bull. Amer. Meteor. Soc.*, vol. 74, pp. 2331-2342.

Soden, B. J. and F. P. Bretherton, 1993: Upper Tropospheric Relative Humidity from the GOES 6.7 μm Channel: Method and Climatology for July 1987, *J. Geophys. Res.*, vol. 98, pp. 16669-16688.

Udelhofen, P. M. and D. L. Hartmann, 1994: Influence of Tropical Cloud Systems on the Relative Humidity in the Upper Troposphere, *J. Geophys. Res.*, in press.

Waters, J. W., L. Froidevaux, W. G. Read, G. L. Manney, L. S. Elson, D. A. Flower, R. F. Jarnot, and R. S. Harwood, 1993: Stratospheric ClO and Ozone from the Microwave Limb Sounder on the Upper Atmosphere Research Satellite, *Nature*, vol. 362, pp. 597-602.

Waters, J. W., 1993: chapter 8 in *Atmospheric Remote Sensing by Microwave Radiometry*, 572 pp., edited by M. A. Janssen, John Wiley and Sons, Inc, New York.

WU, X., J. J. Bates, and S. S. Khalsa, 1993: A Climatology of the Water Vapor Band Brightness Temperatures from NOAA Operational Satellites, *J. Climate*, vol. 6, pp. 1282-1300.

W. G. Read, J. W. Waters, D. A. Flower, L. Froidevaux, and R. F. Jarnot, Mail Stop 183-701, Jet Propulsion Laboratory, 4800 Oak Grove Dr, Pasadena, Ca. 91109.

D. L. Hartmann, University of Washington, Department of Atmospheric Science, Code AK-40, Seattle, Wa. 98195.

R. S. Harwood, University of Edinburgh, Department of Meteorology, James Clerk Maxwell Building, Edinburgh, EH9 3JZ, Scotland.

R. B. Rood, Code 910.3, NASA/GSFC, Greenbelt, MD 20771

(Received: Month? day?, 1994;

Paper number XXXX.

Read et al.: MLS Upper Tropospheric H₂O.

Read et al.: MLS Upper Tropospheric H₂O.

Read et al.: MLS Upper Tropospheric. H₂O.

Fig. 1. See figure 1

Fig. 2. See figure 2

Fig. 3. See figure 3

Fig. 4. See figure 4

Fig. 5. See figure 5

Fig. 6. See figure 6

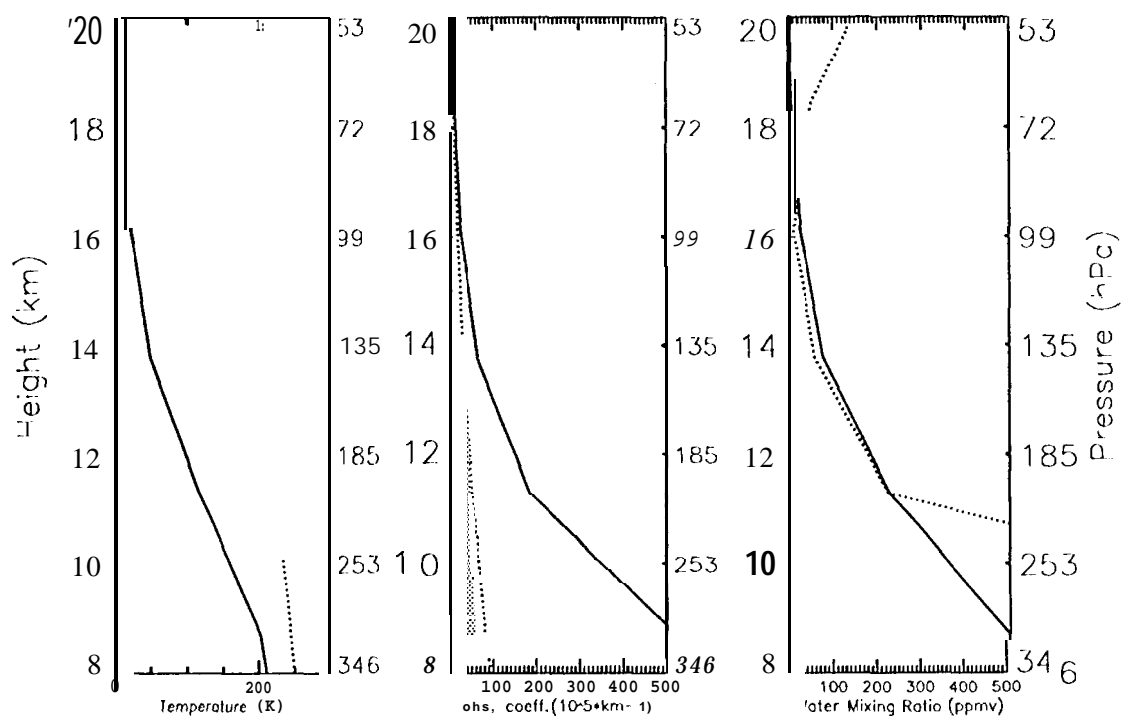


Figure 1: Illustration of upper tropospheric water vapor retrieval scheme used here. The left panel shows measured radiances (solid line) and NMC temperatures (dotted line) interpolated onto an equally spaced \log_{10} -pressure altitude grid. The center panel shows conversion to absorption coefficient (solid line). The contribution due to cirrus can assume any value inside the shaded region whose rightmost extent is indicative of a 120 km horizontally thick, and 0.1 g m^{-3} cirrus. The dotted line is the absorption coefficient from the empirically-derived collision-induced dry air absorption. The right panel is the retrieved water vapor profile (solid line) after subtracting the dry air continuum but ignoring any cirrus contributions. A 100% ice relative humidity curve (dotted line) shown for comparison. This example is for a tropical measurement having high water content.

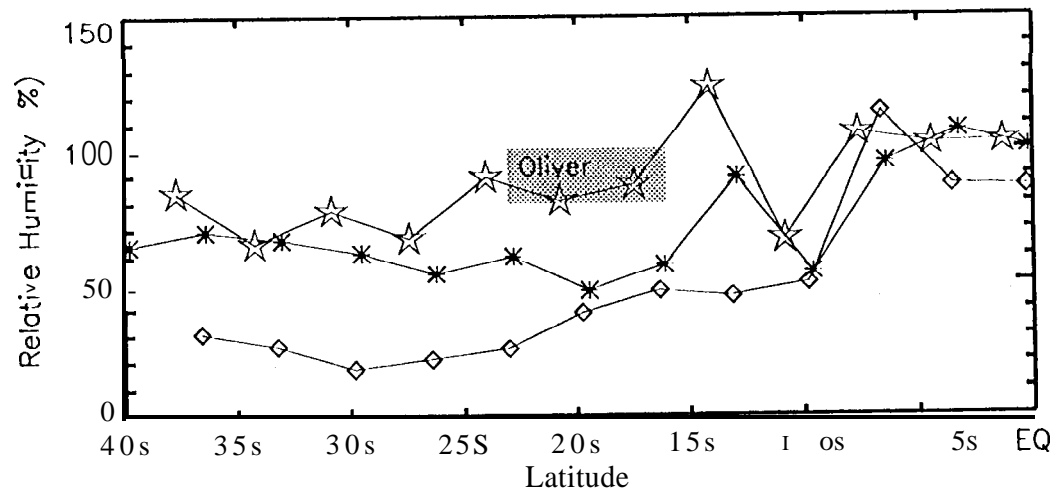


Figure 2: Retrieved relative humidity along three adjacent M 1,S measurement tracks within 0-40° S latitude and 130°13'-170°11' longitude at 215 hPa on 8 February 1993. The "Oliver" cyclone location is shaded and the track denoted by stars goes through it. The track depicted with diamonds is to the east over ocean, and asterisks depict the track to the west and mostly along the Australian east coast.

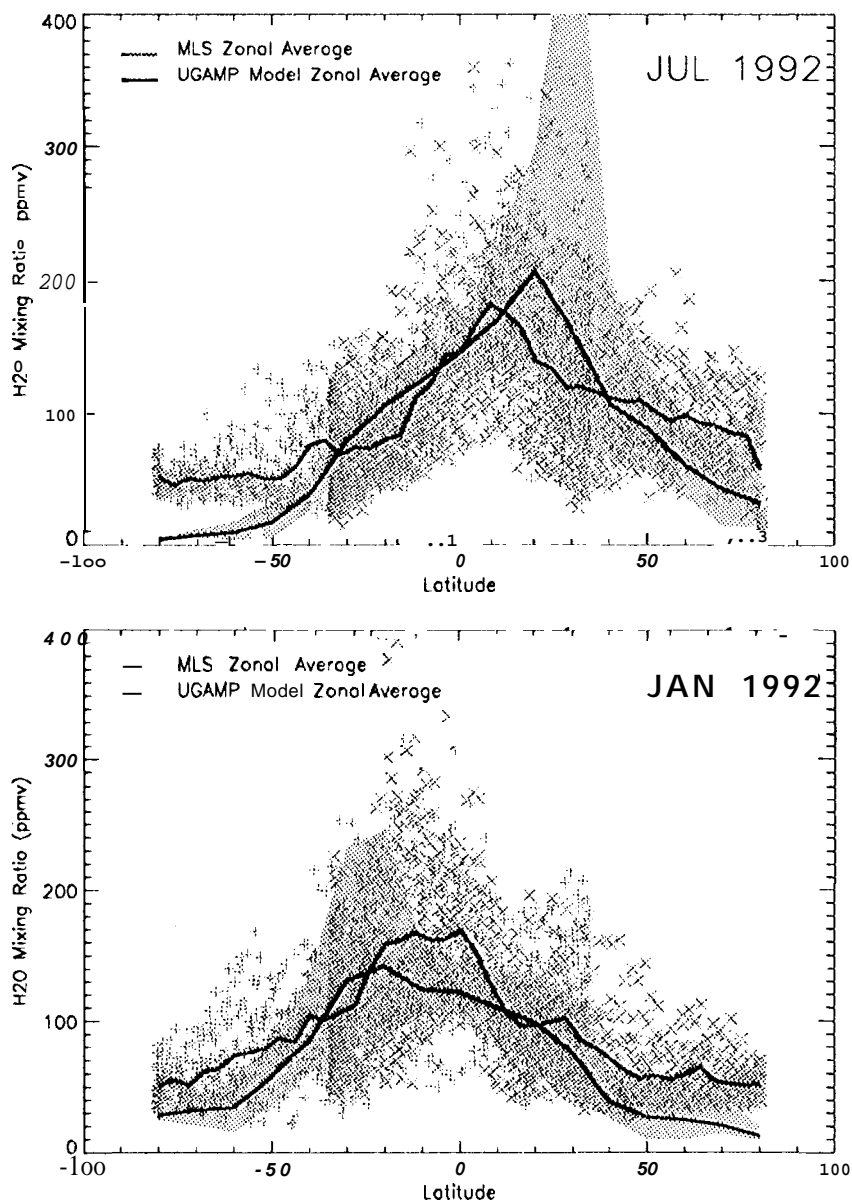


Figure 3: January and July H₂O versus latitude. Green x and + are individual MLS measurements from two days, Red shaded area indicates the range of values predicted by the UKUGAMP model.

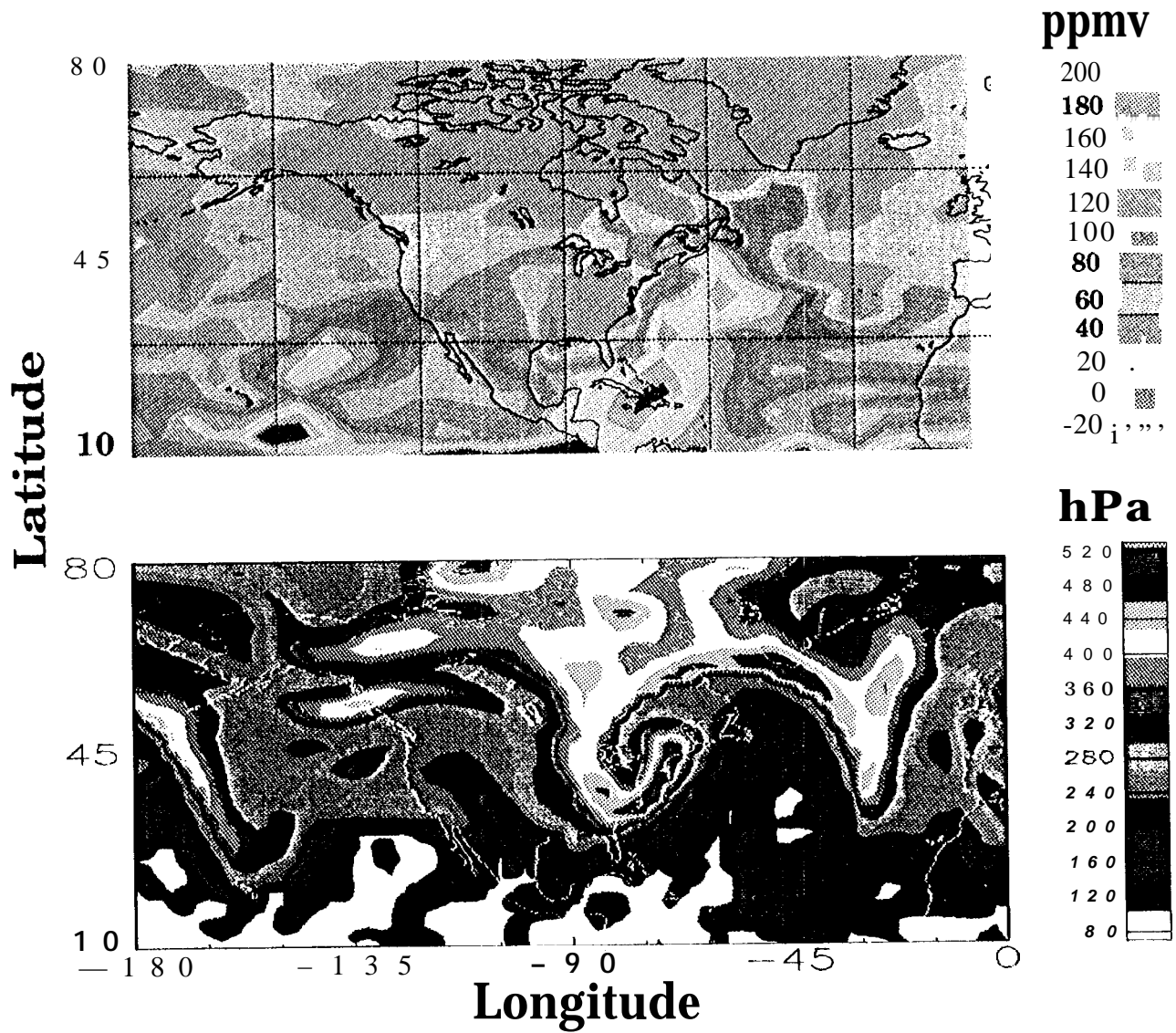
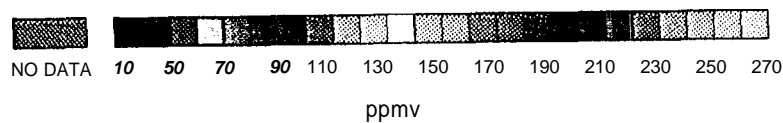
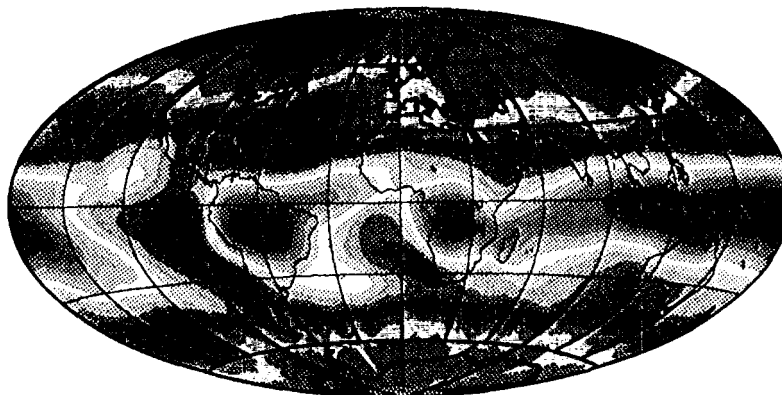


Figure 4: Top panel shows MLS 215 hPa water vapor on March 14 1993 when the eastern coast of the US was experiencing a severe blizzard, The bottom panel shows the tropopause pressure for the same day from the GSFC assimilation model.

UARS MLS215hPa Water Vapor
DJF 1991-1994



ISCCP High Thick Cloud Amount
DJF 1983-1990

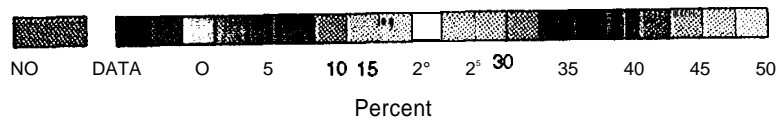
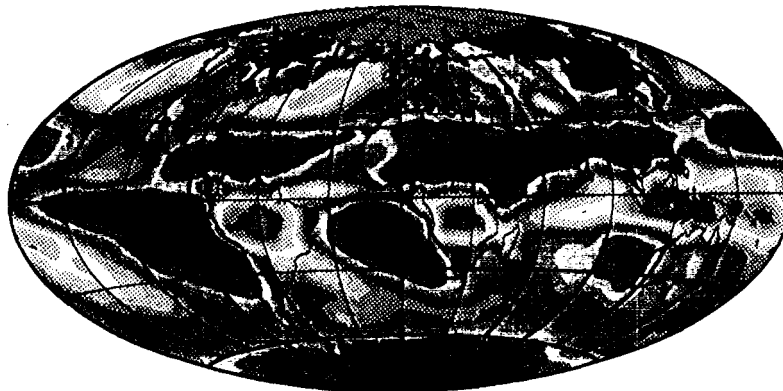
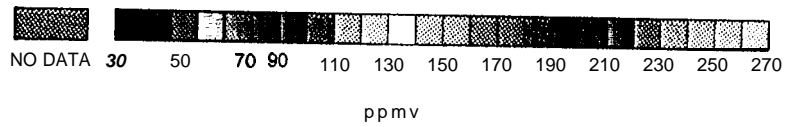
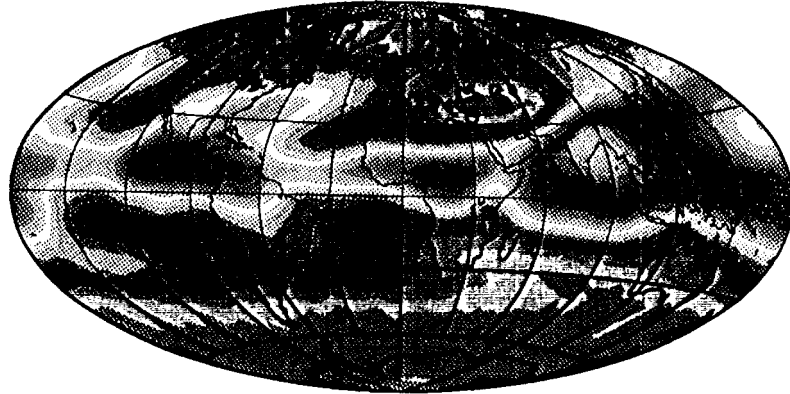


Figure 5: Top panel shows the 215 hPa MLS water vapor climatology for December- February which uses measurements made from 1991 to 1993 binned into $4^\circ \times 4^\circ$ latitude/longitude boxes. The bottom panel shows the December-February, 1983-1990 ISCCP fractional high thick (altitude above 440 hPa. and visible optical depth greater than 9.38) cloud cover climatology map.

UARS MLS 215hPa Water Vapor
JJA 1992-1993



ISCCP High Thick Cloud Amount
JJA 1933-1990

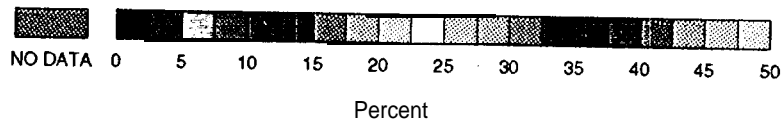


Figure 6: Top panel shows the 215 hPa MLS water vapor climatology for June-August which uses measurements made from 1992 to 1993 binned into $4^\circ \times 4^\circ$ latitude/longitude boxes. The bottom panel shows the June-August, 1983-1990 ISCCP fractional high thick (altitude above 440 hPa, and visible optical depth greater than 9.38) cloud cover climatology map.